

Photoluminescent Properties of Nanorods and Nanoplates $Y_2O_3:Eu^{3+}$

Ana Paula de Moura · Larissa Helena de Oliveira · Elaine Cristina Paris ·
Máximo Siu Li · Juan Andrés · José Arana Varela · Elson Longo ·
Ieda Lucia Viana Rosa

Received: 28 September 2010 / Accepted: 29 December 2010
© Springer Science+Business Media, LLC 2011

Abstract Nanorods and nanoplates of $Y_2O_3:Eu^{3+}$ powders were synthesized through the thermal decomposition of the $Y(OH)_3$ precursors using a microwave-hydrothermal method in a very short reaction time. These powders were analyzed by X-ray diffraction, field emission scanning electron microscopy, Fourier transform Raman, as well as photoluminescence measurements. Based on these results, these materials presented nanoplates and nanorods morphologies. The broad emission band between 300 and 440 nm ascribed to the photoluminescence of Y_2O_3 matrix shifts as the procedure used in the microwave-hydrothermal assisted method changes in the $Y_2O_3:Eu^{3+}$ samples. The presence of Eu^{3+} and the hydrothermal treatment time are responsible for the band shifts in $Y_2O_3:Eu^{3+}$ powders, since in the pure Y_2O_3 matrix this behavior was not observed. $Y_2O_3:Eu^{3+}$ powders also show the characteristic Eu^{3+} emission lines at 580, 591, 610, 651 and 695 nm, when excited at 393 nm. The most intense band at 610 nm is responsible for the Eu^{3+} red emission in these materials, and the Eu^{3+} lifetime for this transition presented a slight

increase as the time used in the microwave-hydrothermal assisted method increases.

Keywords Photoluminescence · Nanorods · Nanoplates · Yttrium oxide · Europium · Microwavehydrothermal method

Introduction

Over the past decades there has been a growing interest in the preparation, characterization, and optimization of a variety of compounds doped with trivalent rare earth ions for the development of new or improved optoelectronic devices, which include solid state lasers, infrared optical fiber amplifiers, luminescent lamps, optical data storage, 3D displays, etc. [1–5].

Yttrium oxide (Y_2O_3) possesses excellent properties and it has many attractive applications such as laser and infrared optical materials [6–9]. Y_2O_3 is known through its use as the host of rare earth-doped, and, in particular europium (Eu^{3+})-doped Y_2O_3 luminescent presents high luminescence efficiency, high thermostability and chemical durability [2–4]. In addition, one of the most important properties for phosphors application is their chemical purity and low production costs [5]. Therefore, a variety of methods have been used to prepare Y_2O_3 -based phosphors such as spray pyrolysis [10], chemical vapor deposition [11], sol-gel [12], and microwave-assisted [12] to render different kind of Y_2O_3 nanostructures, such as nanotubes [13], nanowires [14], nanorods [15] and nanobelts [16].

Since the determining work of Gedye1 in 1986, the use of microwaves has become a well established technique in chemistry that has found numerous applications in the laboratory as well as in industry [17–19]. Microwave heating is a versatile and widely used tool for preparative

A. P. de Moura · L. H. de Oliveira · E. C. Paris · I. L. V. Rosa (✉)
Departamento de Química, Universidade Federal de São Carlos,
13565-905 São Carlos, SP, Brazil
e-mail: ilvrova@ufscar.br

J. A. Varela · E. Longo
Instituto de Química, Universidade Estadual Paulista,
14800-900 Araraquara, SP, Brazil

M. S. Li
Instituto de Física de São Carlos, USP,
P.O. Box 369, 13560-970 São Carlos, SP, Brazil

J. Andrés
Departament de Química Física y Analítica, Universitat Jaume I,
Castello de la Plana 12071, Spain

63 chemistry and have continually demonstrated its worth
64 within the laboratory setting. A number of books on
65 microwave- assisted synthesis have been published recently
66 [20–22]. The microwave-assisted heating is a greener
67 approach to synthesize materials in a shorter time (from
68 several minutes to a few hours) and with lower power
69 consumption (hundreds of Watts) compared to the conven-
70 tional heating at the same temperatures [23–27], as a
71 consequence of directly and uniformly heating of the
72 components, although other intriguing effects such as
73 changing in the reaction selectivities and increase of
74 reactional rates (microwave catalysis). Consequently,
75 microwave synthesis is becoming quite common in
76 several areas as material sciences, nanotechnology, inor-
77 ganic, organic, biochemical, or pharmaceutical laboratories
78 [10, 28–32].

79 Preparation of $Y_2O_3:Eu^{3+}$ phosphors by the microwave-
80 hydrothermal assisted method (MH) remains surprisingly
81 scarce. Spherical particles of Y_2O_3 and $Y_2O_3:Eu^{3+}$ was
82 prepared using the MH method via hydrolysis in aqueous
83 solution at high-temperature in the presence of urea, and the
84 authors reported that the obtained materials present high
85 crystallinity and high luminescence intensity. Cubic nano-
86 crystalline $Y_2O_3:Eu^{3+}$ with a spherical shape presenting
87 20–30 nm of diameters was successfully prepared using a
88 novel approach, micro-emulsion microwave heating. The
89 obtained materials were excited with 255 nm light, showing
90 bright red emission due to the 4f-4f transitions of Eu^{3+} ions,
91 and the highest photoluminescence (PL) intensity at
92 611 nm was determined in the sample containing about
93 6 mol% Eu^{3+} [12].

94 The present work reports on the PL behaviour of
95 nanorods and nanoplates $Y_2O_3:Eu^{3+}$ powders synthesized
96 via a different MH method for first time here. We also
97 analyzed the influence of the preparation time of the
98 precursors on the optical and morphological properties of
99 these materials, using X-ray diffraction (XRD), field
100 emission microscopy (FEG-SEM), Ultraviolet–visible
101 (UV–vis), absorption and Raman spectroscopy. The PL
102 measurements of the $Y_2O_3:Eu^{3+}$ have been employed on
103 the basis of experimental analysis and it was observed
104 interesting results. The origin of the PL emission excited in
105 different wavelengths (394 and 350 nm) is therefore
106 discussed here in details.

107 Experimental Procedures

Q4 108 Synthesis of the Precursors

109 The synthesis of the precursors was performed using the
110 following procedure: A solution composed by 1.0 mmol of
111 $Y(NO_3)_3 \cdot 8H_2O$ and 80 mL of water were mixed and stirred

for 30 min at room temperature. To this homogenous
solution was then added 20 mL of 0.25 mmol of Eu_2O_3
diluted in HNO_3 . The final pH value of 12.5 was adjusted
using a 5.00 M NaOH solution. After stirring for about
30 min, the resulted mixture was transferred to a Teflon-
lined stainless autoclave. This autoclave was then sealed
and placed into a MH (2.45 GHz, maximum power of
800 W). The MH conditions were kept at 140 °C for 10, 20
and 40 min. The white powders, obtained through these
different times, were labeled, respectively, as **P1**, **P2** and
P4, collected, washed with water, and then dried at 60 °C
for 8 h under atmospheric air in a conventional furnace.

Synthesis of Y_2O_3 and $Y_2O_3:Eu^{3+}$ Powders 124

The $Y_2O_3:Eu^{3+}$ powders were obtained from thermal
decomposition of the precursors **P1**, **P2** and **P4**. These
precursor powders were placed in ceramic crucibles and
heated in a microwave sintering furnace at 500 °C for
20 min. These calcinated white powders were respectively
called as **Y1**, **Y2** and **Y4** samples. The procedure used for
the obtention of pure Y_2O_3 powders was the same as for
 $Y_2O_3:Eu^{3+}$ powders, resulting in the samples **NY1**, **NY2**
and **NY4**.

Characterization 134

Y1, **Y2** and **Y4** as well as **NY1**, **NY2** and **NY4** samples
were characterized by powder X-ray diffraction using a
Rigaku-DMax 2500PC, Japan, with Cu $K\alpha$ radiation, $\lambda =$
1.540598 Å, in the 2θ range from 5 to 75° using an
increment of 0.02°/min. The PL was measured with a
Thermal Jarrel-Ash Monospec 27 monochromator and a
Hamamatsu R446 photomultiplier. The 350.7 nm exciting
wavelength of a krypton ion laser (Coherent Innova) was
used, with the nominal output power of the laser power
kept at 200 mW. All the measurements were taken at room
temperature. The excitation and emission spectra of the
 $Y_2O_3:Eu^{3+}$ samples were measured in a Jobin Yvon-
Fluorolog 3 spectrofluorometer at room temperature using
a 450 W xenon lamp as excitation energy source. Lifetime
data of the $Eu^{3+} \ ^5D_0 \rightarrow \ ^7F_2$ transition in the $Y_2O_3:Eu^{3+}$
samples were evaluated from the decay curves using the
emission wavelength set at 612 nm and excitation wave-
length set at 393 nm. The morphologies and sizes of the
samples were observed using a field emission gun scanning
electron microscopy (FEG-SEM) - Jeol JSM 6330F.

Results and Discussion 155

Figure 1(a) presents the XRD patterns of the precursors,
represented by the sample **P1**, since **P2** and **P4** diffracto-

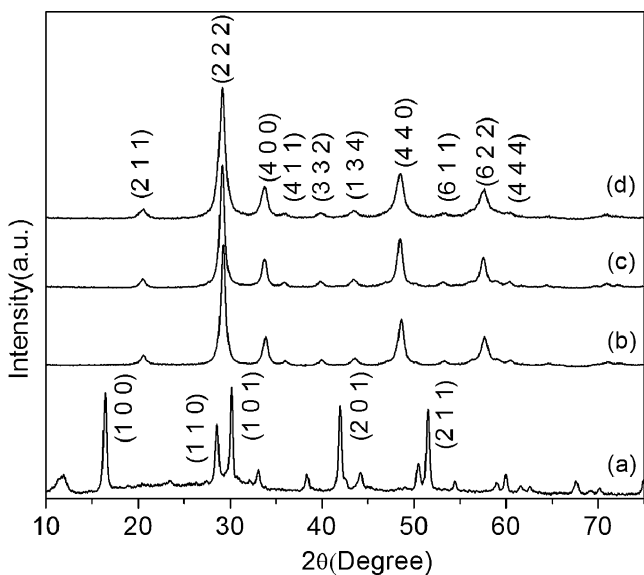


Fig. 1 XRD patterns of the as-prepared **P1** powder (a); and the $Y_2O_3:Eu^{3+}$ powders heated at 500 °C for 20 min in a microwave oven (b) **Y1**, (c) **Y2** and (d) **Y4**

grams have the same feature. Figure 1(b, c and d) shows the XDR patterns of the $Y_2O_3:Eu^{3+}$ powders, **Y1**, **Y2** and **Y4**, respectively. In the diffractogram of **P1** (Fig. 1(a)), it was not observed any diffraction peak ascribed to the Y_2O_3 crystalline phase. The precursor composition is mainly associated to yttrium hydroxide ($Y(OH)_3$). This conclusion was possible, since this diffractogram presents the characteristic peaks of this matrix according to JCPDS data file (# 83-2042). However, in the XDR patterns of the $Y_2O_3:Eu^{3+}$ powders (Fig. 1(b, c and d)), was observed the diffraction peaks ascribed to a pure body-centered cubic Y_2O_3 phase at $2\theta=20.5^\circ, 29.1^\circ, 33.8^\circ, 36.1^\circ, 39.9^\circ, 43.5^\circ, 48.6^\circ, 53.3^\circ, 57.7^\circ$ and 60.5° , corresponding, respectively, to the (211), (222), (400), (411), (332), (134), (440), (611), (622) and (444), which are in accordance to the JCPDS # 43-1036. From these XDR patterns it was possible to noticed that a heat treatment of 500 °C for only 20 min under a microwave radiation is enable to result in a Yttrium oxide phase, so this is the advantage of this synthetic route, compared to another ones [33–35]. None peaks related to other phases were detected at Fig. 1(b, c and d). So, trough the RXD technique the products **Y1**, **Y2** and **Y4**, prepared by this method, are completely pure in terms of chemical composition.

The synthesis process was then accompanied by the emission and excitation spectra of the Eu^{3+} ion in the doped materials. These spectra data allows us a better understanding on the interactions around the Eu^{3+} ions than the X-ray technique, since RXD technique detects only the long-range interactions, while PL measurements is enable to give information on the Eu^{3+} interactions with the inorganic matrix in a short range distance. The excitation spectra of

Y1, **Y2** and **Y4** samples are presented at Fig. 2. An analysis of the results shows that it was possible to observe narrow bands associated to the $4f^6$ intraconfigurational transitions from the 7F_0 ground state to the 5G_6 excited ones at 362 nm, 5H_4 at 382 nm, and 5L_6 at 394 nm, being the $^7F_0 \rightarrow ^5L_6$ transition one of the most intense as it is normally noticed in inorganic matrix [36]. In this Fig. it was also noticed a broad absorption band that is observed in the range of 250–280 nm (not shown), which was ascribed to charge transfer from Y_2O_3 matrix to Eu^{3+} ions.

The PL emission spectra presented in Fig. 3(a, b, c) show the Eu^{3+} emission line ascribed to transitions from the $Eu^{3+}5D_0$ excited states to the 7F_J ($J=0, 1, 2, 3$ and 4) fundamental ones in the **Y1**, **Y2** and **Y4** powders excited at 393 nm. The most intense band at 610 nm is due to the $^5D_0 \rightarrow ^7F_2$ transition and is called as hypersensitive, being strongly dependent of the Eu^{3+} surrounding, since it is governed by the forced electric dipole mechanism. The emission spectra of all samples presented the $Eu^{3+} ^5D_0 \rightarrow ^7F_J$ ($J=0, 1, 2, 3$ and 4) transitions at 580, 591, 610, 651 and 695 nm, respectively. This indicates that Eu^{3+} site symmetry has no center of inversion. The band emission in the red region (610 nm) is predominant in the PL spectra. The feature of these spectra is similar to data reported in the literature for Eu^{3+} sites into the Y_2O_3 matrix. From the spectroscopic point of view, Eu^{3+} presents an intense red emission in inorganic systems having low symmetry, and normally is used as a probe due to its following characteristic properties (1) the excited states 5D_J ($J=0, 1, 2$ and 3) are well separated ($\sim 12\ 000\ cm^{-1}$) from the ground terms 7F_J ($J'=0, 1, 2, 3, 4, 5$ and 6); (2) both 5D_0 main emitting level and 7F_0 ground state are non-degenerated leading to a single $^5D_0 \rightarrow ^7F_0$ transition when

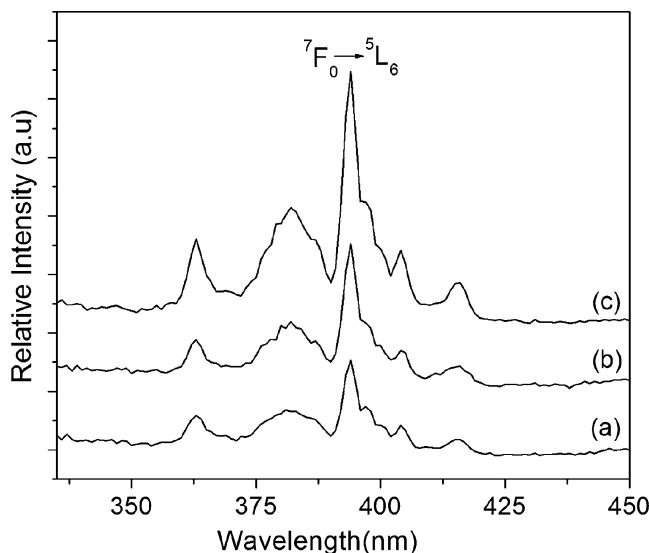


Fig. 2 Excitation spectra of $Y_2O_3:Eu^{3+}$ powders heated at 500 °C for 20 min in a microwave oven (a) **Y1**, (b) **Y2** and (c) **Y4**

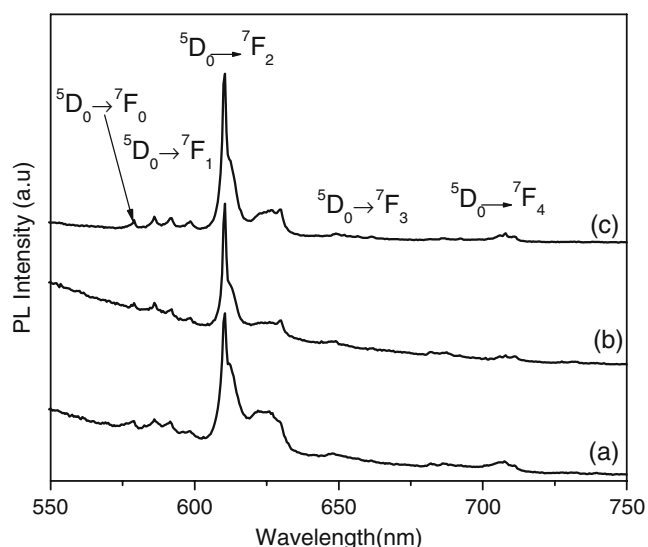


Fig. 3 Emission spectra of $Y_2O_3:Eu^{3+}$ powders heated at 500 °C for 20 min in a microwave oven (a) **Y1**, (b) **Y2** and (c) **Y4**. All samples were excited with a xenon lamp in 394 nm, at room temperature

223 the Eu^{3+} ions occupy C_s , C_n or C_{nv} site symmetries,
 224 therefore the ${}^5D_0 \rightarrow {}^7F_0$ transition usually appears as a
 225 single peak in the photoluminescence spectra as the Eu^{3+}
 226 ions occupy identical site symmetries [37–40]. This fact
 227 facilitates the interpretation of the spectral data and
 228 provides informations on the eventual existence of more
 229 than one site symmetry occupied by the Eu^{3+} ion; (3) The
 230 ${}^5D_0 \rightarrow {}^7F_1$ transition can be used as a reference transition
 231 because it is allowed by forced magnetic dipole, and
 232 consequently the intensity of this transition is not consid-
 233 erably altered by the Y_2O_3 matrix perturbing crystal field;
 234 (4) long luminescence decay time of around milliseconds
 235 for the 5D_0 level and (5) exceptionally large Stokes shifts
 236 when the emission spectra are obtained through the direct
 237 excitation of the $Eu^{3+} {}^5L_6$ level, at around 394 nm, like in
 238 this case (see Fig. 2), or through the excited state that is
 239 located at higher energies belonging to the host matrix or,
 240 in some cases, to organic ligands. The insert of Fig. 3
 241 shows the photoluminescence spectrum of the precursor P1,
 242 as illustration, obtained at the same conditions as those at
 243 Fig. 3(a, b and c). As we can see, the P1 photoluminescence
 244 spectrum presents Eu^{3+} emission bands that were in
 245 accordance with the $Y(OH)_3 Eu^{3+}$ doped [34].

246 It was noticed a decrease in the Eu^{3+} emission intensity
 247 when the samples were submitted to the microwave
 248 radiation from 10 to 20 min, indicating a structural
 249 rearrangement around Eu^{3+} . As the time of exposure to
 250 microwave radiation increases from 20 to 40 min, however,
 251 it was observed an increase in the relative intensity of the
 252 Eu^{3+} characteristic bands (Fig. 3(a, b and c)). During the
 253 sintering process the tendency to increase the emission
 254 intensity is due to the fact that OH^- groups around the Eu^{3+}

255 are being replaced by the O^{2-} bonds of the $Y_2O_3:Eu^{3+}$
 256 matrix. OH^- groups have different vibration levels, whose
 257 energies are located between the 5D_0 excited level and the
 258 7F_6 ground one of the Eu^{3+} ions in this framework. So, as
 259 these groups are substituted by the Eu^{3+} it is noticed the
 260 decrease in the emission quenching caused by the non-
 261 radiative processes decrease [41].

262 The decay curves of the $Eu^{3+} {}^5D_0 \rightarrow {}^7F_2$ transition
 263 excited at 393 nm with the emission set at 613 nm,
 264 presented a non-exponential feature and when fitted in a bi-
 265 exponential function, resulted in lifetimes of 1.19 ms for
 266 **Y1**, 1.70 ms for **Y2** and 1.76 ms for the **Y4** sample,
 267 determined from the first part of the curves, respectively. As
 268 the time of heat treatment enhances, it was noticed an
 269 increase in the lifetime of the Eu^{3+} emission, indicating the
 270 incorporation of this ion by the Y_2O_3 matrix.

271 Raman spectroscopy can be used to characterize the
 272 phonon energy of these materials. The order–disorder
 273 degree in a short range of the crystalline structure was
 274 studied through the spectroscopic analysis. Fig. 4(a, b and
 275 c) displays, respectively, the Raman spectra of $Y_2O_3:Eu^{3+}$
 276 powders **Y1**, **Y2** and **Y4** after heated at 500 °C for 20 min
 277 in the microwave oven. From these Raman spectra were
 278 verified the **Y1**, **Y2** and **Y4** samples presented the Raman
 279 active mode at 372, 461 and 583 cm^{-1} , which are related to
 280 the cubic Y_2O_3 phase according to recent report on [42, 43]
 281 Raman spectrum of Y_2O_3 . These data are also in accord-
 282 ance to the XDR patterns. As the time of exposure to the
 283 microwave radiation increases the relative intensity of the
 284 Raman active modes enhances, indicating an increase in the
 285 degree of structural order at short-range.

286 To a better understanding of the PL properties and its
 287 dependence on the structural order–disorder in the Y_2O_3
 288 lattice, the PL emission spectra of the $Y_2O_3:Eu^{3+}$ powders

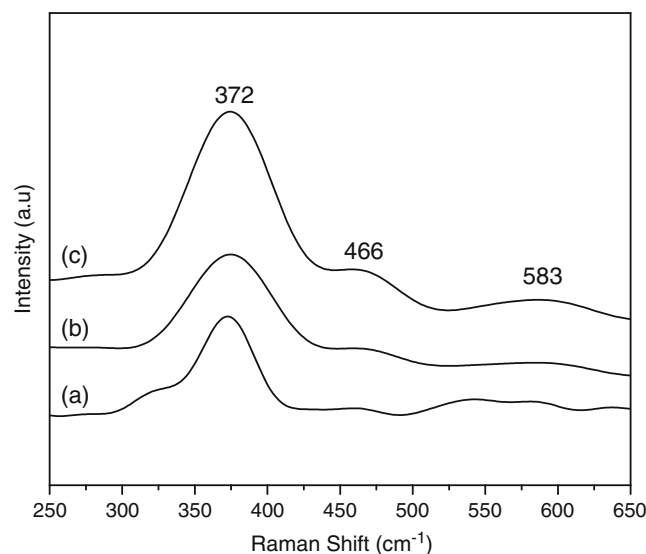


Fig. 4 RAMAN spectra of the **Y1**(a), **Y2**(b) and **Y4** (c) samples

289 **Y1, Y2 and Y4** were performed at room temperature, using
 290 an excitation of a krypton laser source at 350.7 nm. These
 291 spectra are presented in Fig. 5a, where it was also observed
 292 a broad emission band ascribed to the emission of the Y_2O_3
 293 matrix for all samples, as well as the characteristic bands of
 294 Eu^{3+} ions. In the PL spectrum of the **Y1** sample, the broad
 295 band is noticed from 300 to 440 nm, presenting an emission
 296 intensity maximum at 423 nm, while **Y2** sample presented a
 297 maximum at 429 nm (violet region). In the PL emission
 298 spectrum of the **Y4** sample, this broad band was shifted to a
 299 higher wavelength, with a maximum at 446 nm (blue
 300 region). This shift of the maximum intensity of the broad
 301 band can be associated to a larger charge density around
 302 Eu^{3+} compared to the Y^{3+} sites caused by the lanthanide
 303 contraction. The variation of the hydrothermal treatment
 304 time can modify the material surface promoting the
 305 appearing of deep defects in the $Y_2O_3:Eu^{3+}$ matrix, which

is also responsible for the broad band shift to higher
 wavelength (red region). The PL emission spectra of pure
 Y_2O_3 powders, **NY1, NY2 and NY4**, are presented in the
 Fig. 5b. These broad emission bands are due to charge
 transfer into the inorganic matrix, and no shift was
 observed with the microwave performance used in this
 study. In accordance with these results, it is clear that both
 the presence of Eu^{3+} and the hydrothermal treatment time
 are responsible for the band shifts, since in the samples
NY1, NY2 and NY4 (Fig. 5b) this behavior was not
 observed.

Figure 6 shows the FEG-SEM micrographies of the **Y1**
 (A and B), **Y2**(C and D) and **Y3** (E and F) samples,
 respectively. From these micrographies, it was verified that
 the particles are agglomerated and polydispersed. These
 systems presented two categories of morphologies. Some
 particles are nanowires-like and some others are
 nanoplates-like, then this phenomenon can be associated
 with the exposure time under microwave radiation. It was
 also observed homogeneity in the sizes of **Y2**, which
 presented an average length of around 276–297 nm and an
 average width of 33–34 nm. The **Y1** sample presented an
 average length of 560–874 nm and an average width of
 50 nm, while the **Y4** sample presented an average length of
 178–184 nm and an average width of 28 nm, corroborating
 with a nanoscale range.

Into the Teflon autoclave, firstly, the microwave radi-
 ation interacts with the permanent dipole of the liquid phase.
 This interaction leads to a vibration on the charged particles
 or molecules, resulting in a rapid heating of the chemical
 solution, promoting, consequently, the formation of the Y
 (OH)₃ precursor particles in a quickly way. The increase of
 the temperature by the microwave radiation promotes the
 dissociation of some Y(OH)₃ particles in Y^{3+} and OH^-
 ions. However, the thermodynamic conditions and the
 electrostatic interactions between these ions favor the
 recrystallization process. Moreover, the microwave radi-
 ation is able to accelerate the solid particles to elevated
 velocities, leading to an increase of the interparticle
 collisions, inducing the effective fusion of these particles
 at the point of collision. These mechanisms are responsible
 for the fast nucleation of the Y_2O_3 grains, as well as the
 aggregation of several small particles [44]. This phenom-
 enon was verified by the formation of aggregated particles
 in different morphologies, being some of them nanowires
 and others nanoplates-like, as observed at Fig. 6(a), after
 10 min of microwave heating. As the reaction proceeds
 from 10 to 20 min, some amorphous particles are dissolved
 and are, after that, condensed beginning the appearance of
 ultrafine wires of Y_2O_3 , presented at Fig. 7(c). After 40 min
 of microwave radiation exposure, it is supposed that occur
 the precursor recrystallization, and through this process we
 suggest the coalescence of the precursor particles, giving

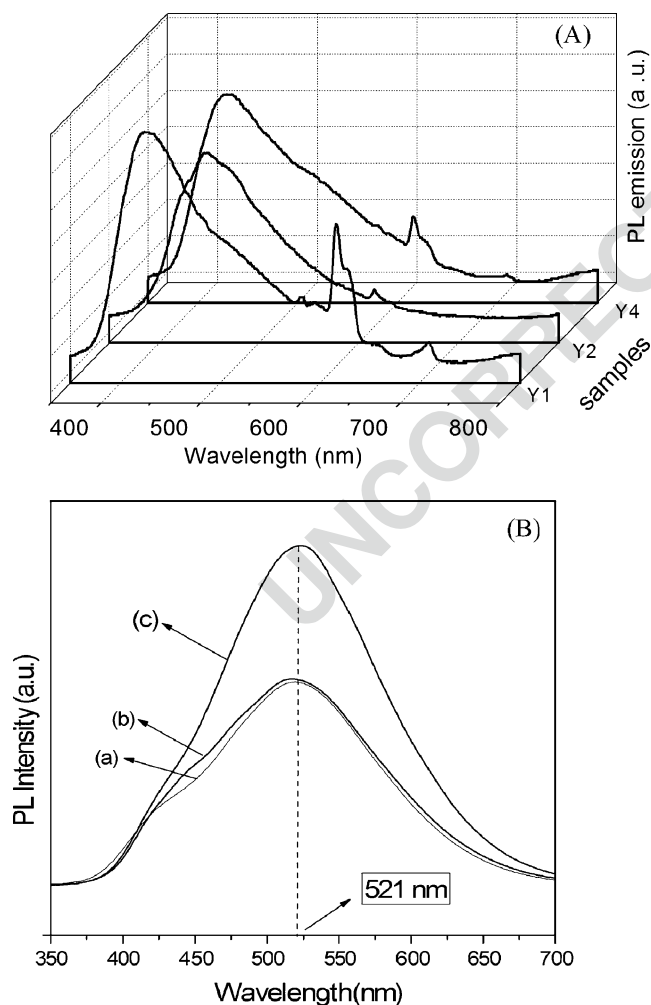
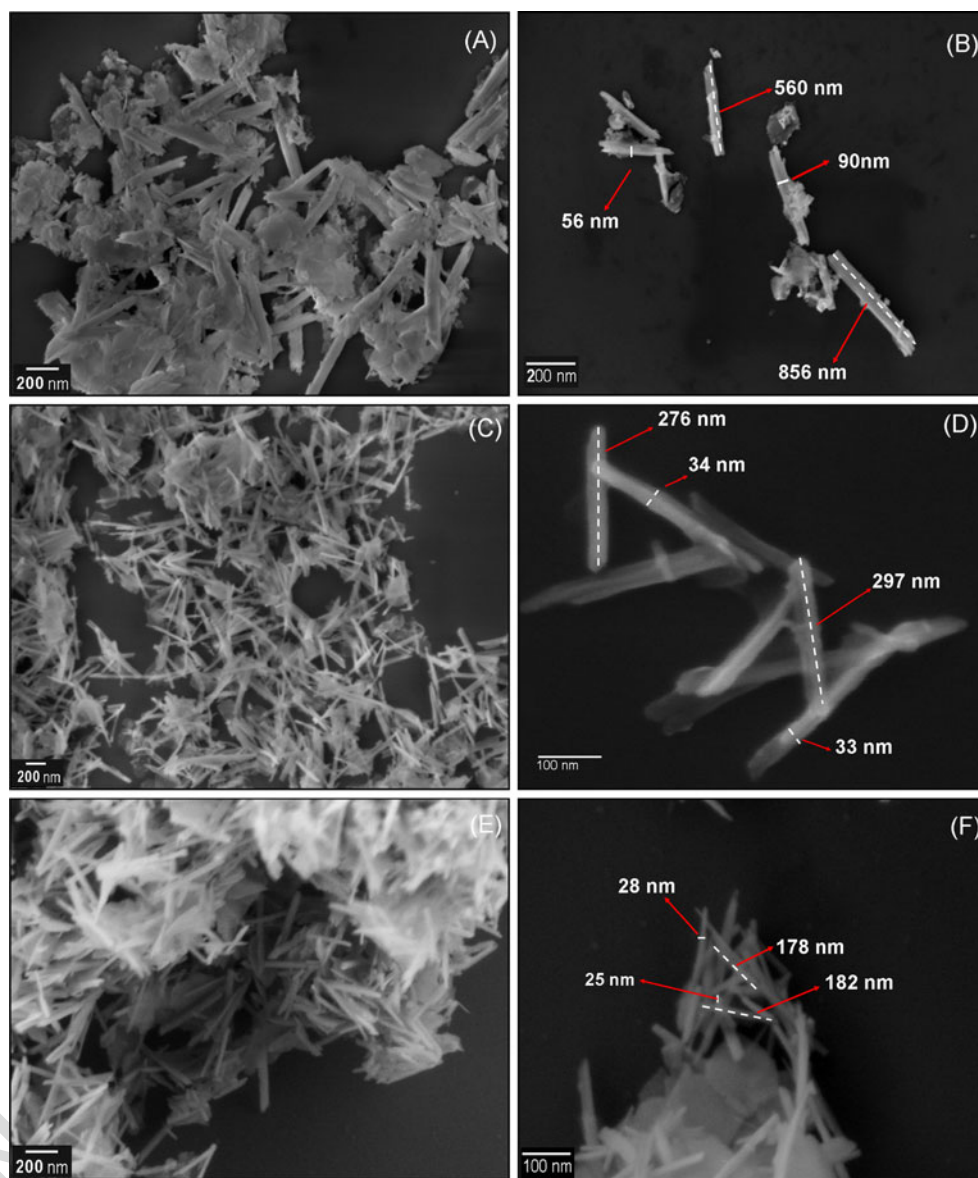


Fig. 5 (A) PL spectra of the $Y_2O_3:Eu^{3+}$ powders microwave heated at 500 °C for 20 min for **Y1, Y2 and Y4**. (B) PL spectra of the Y_2O_3 samples heated at 500 °C for 20 min microwave oven (a) **NY1**, (b) **NY2** and (c) **NY4**. All samples were excited with krypton ion laser of 350.7 nm, at room temperature

Fig. 6 FEG-SEM micrographies of $Y_2O_3: Eu^{3+}$ of the powders heated at 500 °C for 20 min at microwave oven (a and b) Y_1 , (c and d) Y_2 and (e and f) Y_4



359 rise mainly to the Y_2O_3 phase (Fig. 6(e)). During the MH
 360 processing the reactional autoclave was not stirred. So, the
 361 electrostatic interactions between the ions increase, promoting
 362 aggregations that lead to the formation of Y_2O_3
 363 seeds. It was also possible to observe, in this case, the
 364 presence of particles with two kinds of morphologies. The
 365 schematic representation of the growth mechanism of the
 366 Y_2O_3 particles by the MH proceeding is exposed at Fig. 7.

367 Conclusions

368 The synthesis process utilizing the MH method in a short
 369 time was successful in the obtention of the precursors
 370 giving rise to both pure and Eu^{3+} doped Y_2O_3 . These
 371 materials presented two different kinds of morphologies,
 372 nanoplates and nanorods. The broad emission band be-

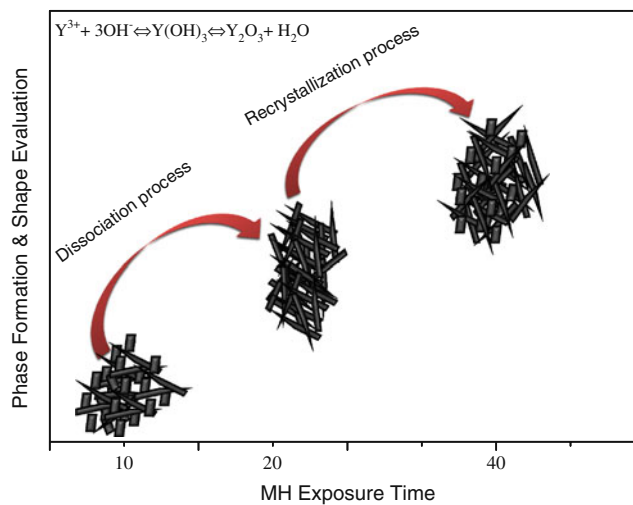


Fig. 7 Schematic representation of the growth mechanism of the Y_2O_3 particles by the MH method

373 tween 300 and 440 nm ascribed to the Y_2O_3 PL shifts as the
 374 MH procedure changes only in the Eu^{3+} doped materials.
 375 $Y_2O_3:Eu^{3+}$ powders show the characteristics Eu^{3+} emission
 376 lines due to the 5D_0 to the 7F_j ($J=0, 1, 2, 3$ and 4)
 377 transitions at 580, 591, 610, 651 and 695 nm, when were
 378 excited at 393 nm. The most intense band at 610 nm
 379 ($^5D_0 \rightarrow ^7F_2$) is responsible for the Eu^{3+} red emission in these
 380 materials. The band emission in the red region (610 nm) is
 381 predominant in the PL emission spectra. From the spectro-
 382 scopic point of view, Eu^{3+} ion gave us valuable information
 383 since it is a structural probe.

384 References

- 386 1. Ronda CR (1997) Recent achievements in research on phosphors
 387 for lamps and displays. *J Lumin* 72:49–54
- 388 2. Kitai AH (2003) Oxide phosphor and dielectric thin films for
 389 electroluminescent devices. *Thin Solid Films* 445:367–376
- 390 3. Wakefield BG, Holland E, Dobson PJ, Hutchison TL (2001)
 391 Luminescence properties of nanocrystalline $Y_2O_3:Eu^{3+}$. *Adv*
 392 *Mater* 13:1557–1560
- 393 4. Vanetsev AS, Butkina EP, Baranchikov AE, Shaporev AS,
 394 Dzuban AV, Soldatov MA, Hao Z, Tret'yakov YD (2009)
 395 Microwave-assisted synthesis of spherically shaped monodisperse
 396 Y_2O_3 and $Y_2O_3:Eu$ powders. *Dokl Chem* 424:35–38
- 397 5. Serra OA, Cicillini SA, Ishiki RR (2000) A new procedure to obtain
 398 Eu^{3+} doped oxide and oxosalt phosphors. *J Alloy Comp* 303:316
- 399 6. Ikegami T, Li J-G, Mori T, Moriyoshi Y (2002) Fabrication of
 400 transparent Yttria ceramics by the low-temperature synthesis of
 401 Yttrium hydroxide. *J Am Ceram Soc* 85(7):1725–1729
- 402 7. Zheng JX, Ceder G, Maxisch T, Chim WK, Choi WK (2006) Factors
 403 determining the shape of the temperature dependence of the
 404 spontaneous magnetization of a ferromagnet. *Phys Rev B* 73:104101
- 405 8. Zhang J, An L, Liu M, Shimai S, Wang S (2009) Sintering of Yb^{3+} :
 406 Y_2O_3 transparent ceramics in hydrogen atmosphere. *J Eur Ceram*
 407 *Soc* 29:305–309
- 408 9. Jollet F, Noguera C, Thromat N, Gautier M, Duraud JP (1990)
 409 Electronic structure of Yttrium oxide. *Phys Rev B* 42(12):7587
- 410 10. Sun LD, Yao J, Liu C, Liao C, Yan CH (2000) Rare earth
 411 activated nanosized oxide phosphors: synthesis and optical
 412 properties. *J Lumin* 87–89:447–450
- 413 11. Lee MH, Oh SG, Yi SC (2000) Preparation of Eu-Doped Y_2O_3
 414 luminescent nanoparticles in nonionic reverse microemulsions. *J*
 415 *Colloid Interface Sci* 226:65–70
- 416 12. Wu GS, Lin Y, Yuan XY, Xie T, Cheng BC, Zhang LD (2004) A
 417 novel synthesis route to $Y_2O_3:Eu$ nanotubes. *Nanotechnology*
 418 15:568–571
- 419 13. Zhang JL, Hong GY (2004) Preparation and characterization of
 420 the $Y(2)O(3): Eu^{3+}$ nanowires. *Chem J Chin Univ-Chinese* 25
 421 (8):1416–1418
- 422 14. Li Q, Feng C, Jiao Q, Guo L, Liu C, Xu HB (2004) Shape-
 423 controlled synthesis of yttria nanocrystals under hydrothermal
 424 conditions. *Phys Status Solidi, A* 201(14):3055–3059
- 425 15. He Y, Tian Y, Zhu Y (2003) Large-scale synthesis of luminescent
 426 $Y_2O_3:Eu$ nanobelts. *Chem Lett* 32(5):862–863
- 427 16. Whitefield PS, Davidson IJ (2000) Microwave synthesis of
 428 $Li_{1.025}Mn_{1.975}O_4$ and $Li_{1+x}Mn_{2-x}O_4-yFy$ ($x=0.05, 0.15; y=$
 429 $0.05, 0.1$). *J Electrochem Soc* 147(12):4476–4484
- 430 17. Gedye R, Smith F, Westaway K, Ali H, Baldisera L, Laberge L,
 431 Rousell J (1986) The use of microwave ovens for rapid organic
 432 synthesis. *Tetrahedron Lett* 27:279–282
18. Larhed M, Moberg C, Hallberg A (2002) Microwave-accelerated
 homogeneous catalysis in organic chemistry. *Acc Chem Res*
 35:717–727
19. Kingston HM, Haswell JS (1997) Microwave-enhanced chemis-
 try. American Chemical Society, Washington
20. Loupy A (ed) (2006) Microwaves in organic synthesis, 2nd edn.
 Wiley-VCH, Weinheim
21. Kappe CO, Stadler A (2005) Microwaves in organic and
 medicinal chemistry. Wiley-VCH, Weinheim
22. Lidström P, Tierney JP (eds) (2005) Microwave-assisted organic
 synthesis. Blackwell, Oxford
23. Bohr H, Bohr J (2000) Microwave-enhanced folding and
 denaturation of globular proteins. *Phys Rev E* 61(4):4310–4314
24. Blanco C, Auerbach SM (2002) Microwave-driven zeolite-guest
 systems show athermal effects from nonequilibrium molecular
 dynamics. *J Am Chem Soc* 2002(124):6250
25. Favretto L, Nugent WA, Licini G (2002) *Tetrahedron Lett*
 43:2581–2584
26. Hoz ADL, Diaz-Ortiz A, Moreno A (2004) Selectivity in organic
 synthesis under microwave irradiation. *Curr Org Chem* 8
 (10):903–918
27. Bren M, Janezic D, Bren U (2010) Microwave catalysis revisited:
 an analytical solution. *J Phys Chem A* 114:4197–4202
28. Kappe CO, Stadler A (2005) Microwaves in organic and
 medicinal chemistry. Wiley, Weinheim
29. Obermayer D, Gutmann B, Kappe CO (2009) Microwave
 chemistry in silicon carbide reaction vials: separating thermal
 from nonthermal effects. *Angew Chem Int Ed* 48(44):8321–8324
30. Yao BD, Wang N (2001) Carbon nanotube arrays prepared by
 MWCVD. *J Phys Chem B* 105:11395–11398
31. Zhu Y-J, Wang W-W, Qi R-J, Hu X-L (2004) Microwave –
 assisted synthesis of single-crystalline tellurium nanorods and
 nanowires in ionic liquids. *Angew Chem Int Ed* 43(11):1410–
 1414
32. Tompsett GA, Conner WC, Yngvesson KS (2006) *ChemPhysChem*
 7:29
33. Zhong S, Wang S, Huaping Xu, Hou H, Wen Z, Li P, Wang S,
 Rong X (2009) Spindlelike $Y_2O_3:Eu^{3+}$ nanorod bundles: hydro-
 thermal synthesis and photoluminescence properties. *J Mater Sci*
 44(14):3687–3693
34. Wu X, Tao Y, Gao F, Dong L, Hu Z (2005) Preparation and
 photoluminescence of yttrium hydroxide and yttrium oxide doped
 with europium nanowires. *J Cryst Growth* 277(1–4):643–649
35. Wan J, Wang Z, Chen X, Li Mu, Qian Y (2005) Shape-tailored
 photoluminescent intensity of red phosphor $Y_2O_3:Eu^{3+}$. *J Cryst*
Growth 284:538–543
36. Teonton EES, Felinto MCFC, Brito HF, Malta OL, Trindade AC,
 Najjar R, Strek W (2004) Synthesis crystalline structure and photo-
 luminescence investigations of the new trivalent rare earth complexes
 (Sm^{3+} , Eu^{3+} and Tb^{3+}) containing 2-thiophenecarboxylate as sensi-
 tizer. *Inorg Chim Acta* 357:451–460
37. Rosa ILV, Oliveira LH, Suzuki CK, Varela JA, Leite ER, Longo E
 (2008) SiO_2-GeO_2 soot preform as a core for Eu_2O_3 nanocoating:
 synthesis and photophysical study. *J Fluoresc* 18:541–545
38. Volanti DP, Rosa ILV, Paris EC, Paskocimas CA, Pizani PS,
 Varela JA, Longo E (2009) The role of the Eu^{3+} ions in structure
 and photoluminescent properties of $SrBi_{2-n}B_2O_9$ powders. 31
 (6):995–999
39. Buono-Core GF, Li H, Marciniak B (1990) Quenching of excited
 states by lanthanide ions and chelates in solution. *Coord Chem*
Rev 99:55–87
40. Malta OL Brito HF, Menezes JFS, Gonçalves FR, Silva Alves S
 Jr, Farias FS Jr, de Andrade AVM (1997) Spectroscopic properties
 of a new light converting device $Eu(\text{thenoyltrifluoroacetate})_2$
 (dibenzyl sulfoxide). A theoretical analysis based on structural
 data obtained from a sparkle model. *J Lumin* 75:255–268

- 499 41. Serra OA, Nassar EJ, Zapparolli G, Rosa ILV (1994) Organic 506
500 complexes of Eu^{3+} supported in functionalized silica gel: 507
501 highly luminescent material. *J Alloys Compd* 207–208:454– 508
502 456
503 42. Ubaldini A, Carnasciali MM (2008) Raman characterisation of 509
504 powder of cubic RE_2O_3 (RE=Nd, Gd, Dy, Tm, and Lu), Sc_2O_3 510
505 and Y_2O_3 . *J Alloy Comp* 454:374–378 511
513 43. Guo H, Qiao YM (2009) Preparation, characterization, and strong 506
upconversion of monodisperse $\text{Y}_2\text{O}_3:\text{Er}^{3+}$, Yb^{3+} microspheres. 507
Opt Mater 31(4):583–589 508
44. Sczancoski JC, Cavalcante LS, Joya MR, Espinosa JWN, Pizani 509
PS, Varela JA, Longo E (2009) Synthesis, growth process and 510
photoluminescent properties of SrWO_4 powders. *J Colloid* 511
Interface Sci 330(1):227–236 512

UNCORRECTED PROOF